ANISOTROPIC TGO RUMPLING IN EB-PVD THERMAL BARRIER COATINGS UNDER IN-PHASE THERMO-MECHANICAL LOADING

D.S. Balint[a*], S-S Kim[b], Yu-Fu Liu[b], R. Kitazawa[b], Y. Kagawa[b], A.G. Evans[c]
[a]Department of Mechanical Engineering, Imperial College London, London, SW7 2AZ, UK
[b]Research Center for Advanced Science and Technology, The University of Tokyo, 4-6-1 Komaba, Meguro-ku, Tokyo 153-8409, Japan
[c]College of Engineering, University of California, Santa Barbara, CA 93106, USA

Abstract

An EB-PVD Y_2O_3-ZrO_2 thermal barrier system has been tested under in-phase thermo-mechanical fatigue (TMF) conditions with thermal gradient in the through-thickness direction. Undulations in the thermally grown oxide (TGO) were observed to have clear anisotropic behavior with respect to the directions parallel and perpendicular to the loading axis. It was found that undulation wavelengths were nearly the same in both directions but the amplitude in the perpendicular direction was much larger than in the parallel direction. A recent model of TGO rumpling was adapted and used to analyze and explain the origins of the observed rumpling behavior under TMF conditions. Methods for deducing CTE temperature variation and creep properties of the substrate from the experimental strain data are also presented in the course of the derivations. Model results show that tensile stress applied in the loading direction can overcome the compression occurring from lateral expansion during oxide formation, causing undulations to flatten; undulations perpendicular to the loading axis are unaffected. However, ratcheting in the strain cycle experienced by the substrate, which occurs naturally by substrate creep, is necessary for anisotropic rumpling under cyclic stress conditions. Model predictions for constant applied stress are also presented, demonstrating a reversal in the direction of undulation alignment under compression. A threshold stress is identified, in both tension and compression, sufficient to produce appreciable anisotropic rumpling. The model predictions provide a clear mechanism for the anisotropy and further evidence that the lateral expansion strain in the oxide is the driving force for oxide rumpling.

Keywords: Multilayers; physical vapor deposition; ceramics; high temperature deformation; analytical methods.

[*] Corresponding author. Tel.: +44 (0)2075 947084; fax: +44 (0)2075 947010. E-mail address: d.balint@imperial.ac.uk (D.S. Balint).

1. Introduction

Thermal barrier coatings (TBCs) are often used to protect metallic components from high temperature service environments [1-6]. Degradation of TBCs and the underlying substrate can be caused by many factors. In most cases, partial delamination of the TBC is regarded as a critical failure and considerable research has been conducted in order to understand the delamination mechanisms [7-11]. It is now commonly accepted that delamination is strongly affected by thermally grown oxide (TGO) layer growth and rumpling (evolution of periodic undulations). TGO thickening is associated with a lateral expansion strain which is believed to be the driving force for oxide rumpling; as the TGO thickens, the driving force for rumpling increases linearly. Rumpling relieves the TGO of some of its compressive strain energy, but the associated vertical movement can induce tensile stresses in the adjacent layers that may lead to crack nucleation and propagation. Therefore, understanding the undulation behavior of the TGO layer has been, and still is, a very important aspect of predicting and controlling critical TBC failures.

Although rumpling of the TGO layer has been a crucial research subject because of its inherent link to TBC reliability and lifetime [12-19], the undulation behavior is usually studied under cyclic conditions without externally applied loads, or by creep tests under isothermal conditions [18-19]. Reports on the combined effect of thermal cycling and applied loading (hereafter denoted as thermo-mechanical fatigue, or TMF) are scarce. In the present study, attention has been paid to experimental observations and model analysis of undulation behavior in TGO layers under in-phase thermo-mechanical fatigue with a temperature gradient in the through-thickness direction. These observations, and the subsequent analysis, give new insight into how applied loading can affect TGO rumpling, and also relate to actual in-service conditions for TBCs not usually explored.

2. Experimental procedure

An electron beam-assisted physical vapor deposited thermal barrier coating (TBC) system processed by Japan Fine Ceramics Center (JFCC), Nagoya, Japan, was used in this study. The ceramic layer of the TBC was ≈ 200 μm thick 8wt.% Y_2O_3-ZrO_2. The bond coat layer was ≈ 150 μm CoNiCrAlY, which had a chemical composition (wt.%) of 32.0-Ni, 21.0-Cr, 8.0-Al, 0.5-Y and the remainder Co. The substrate was ≈ 3 mm thick Inconel 738LC, and was

comprised of a Ni-base superalloy (16.0-Cr-8.5-Co-3.4-Al-3.4-Ti-1.75-Mo-2.6-W-1.75-Ta-0.85-Nb-0.12-Zr-0.012-B-0.13-C-bal. Ni).

The superalloy substrate was machined into a test coupon, and then bond coat and ceramic layers were simultaneously coated on one side of the substrate. Fig. 1a shows the shape and dimensions of the specimen along with the coordinate system used in the measurements. Cyclic in-phase thermo-mechanical fatigue (TMF) tests were carried out in ambient air using a specially-designed thermo-mechanical testing system. Fig. 1b shows a setup of the TMF system: it consisted of an Instron 8861 machine and specially-designed heating/cooling system. A cylindrical ceramic susceptor plate (Al_2O_3), which was located ~ 10 mm from the surface of specimen, was heated by an RF induction coil with a frequency of 80 kHz and a maximum input power of 10 kW.

The maximum temperature at the surface of the TBC specimen, measured by pyrometer, was set to ≅ 1150 °C. Prior to testing, calibration of the temperature was done using a thermocouple. Preliminary measurements confirmed that the temperature was uniform within the central region of the specimen (approximately 10 mm × 10 mm). Cooling of the specimen was done from the back (i.e. substrate) surface; compressed cooled air blown from a flat nozzle allowed rapid cooling of the specimen. Using this procedure, the surface of the substrate, as measured by a thermocouple, was maintained at ≈ 1000 °C during the isothermal hold at peak temperature, while the peak temperature at the TBC surface was maintained at ≅ 1150 °C. This indicates a steady temperature gradient of $\Delta T \approx$ 150 °C was achieved using the present system. A single cycle of the TMF test lasted 16 min with heating and cooling rates of 5 °C /s and a dwell at the peak temperature of 10 min under constant applied tensile stress and isothermal conditions. The maximum applied stress during the hot stage was either σ_a = 100 or 138 MPa. Here, the applied stress, σ_a, is defined as $\sigma_a \equiv P_a / S_0$ where S_0 is the entire cross sectional area of the coated specimen ($S_0 \cong w(h_{tbc} + h_{bc} + h_s)$, where h_{tbc}, h_{bc} and h_s are the thickness of the ceramic, bond coat and substrate, respectively). Because the TGO layer in the as-coated specimen was very thin, it was neglected in calculating the applied stress. As the superalloy was much thicker than the other layers combined (approximately 8.5 times), the strain resulting from the applied load was dominated by the substrate.

The specimen was fixed to the test machine with water-cooled grips. Flow of heat from the specimen to the fixture occurred during the measurement. However, the effect was small and therefore neglected. Axial strain was measured using an extensometer with a gauge length of

12.5 mm. Tests were continued until complete failure of the TBC system occurred. TBC specimens after failure were observed by optical microscopy. Then they were embedded in an epoxy mount and sections both parallel and perpendicular to the loading axis were carefully polished using a standard metallurgical procedure up to a 0.5 μm diamond paste finish. The polished sections were then imaged by scanning electron microscopy (SEM).

2. Experimental results

Examples of the measured temperature-time (for the TBC surface and back surface of the substrate) and applied stress-time relations of the TMF test are shown in Fig. 2. Both temperature and applied stress are well controlled in the present experimental system. Fig. 3a shows accumulated maximum and minimum axial strains versus the number of cycles, *N*. Here, the maximum cumulative strain at a given cycle, $\varepsilon_{\max}$, was measured at the end of the hold at peak temperature ($T_{tbc} \approx 1150$ °C), and the minimum cumulative strain, $\varepsilon_{\min}$, was measured upon reaching the minimum temperature ($T_{tbc} \approx 300$ °C). The number of cycles to failure was N_F = 27 (Σt_h = 270 min) and N_F = 86 (Σt_h= 860 min) for σ_a = 138 and 100 MPa, respectively. Here, the total hot time, Σt_h, is defined as:

$$\Sigma t_h \equiv N \int_0^{\Delta t} dt = N \Delta t . \qquad (1)$$

where Δt = 10 min is the total time per cycle at the peak temperature (the time elapsed in each heating and cooling of the specimen was 3 min). The substrate was much thicker (approximately 8.5 times) than the TBC layer, so almost the entire applied load was carried by the superalloy substrate. Measurements of axial strain with number of cycles under TMF conditions are consistent with the well-established creep behavior of superalloys at high temperatures [20-23]. Ratcheting behavior clearly appears as shown in one example for σ_a = 138 MPa in Fig. 3b. Under a consistently applied cyclical stress, the ratcheting strain becomes more significant as the number of cycles *N*, and total hot time Σt_h, increase.

TMF was carried out to failure. Fig. 4a shows overall views of the tested specimens at final failure under different applied stresses σ_a. Independent of the applied stress level, the part of the specimen where failure is localized is elongated with slight necking. Many parallel transverse cracks in the hot section of the specimen were observed in the ceramic layer.

However, most of the cracks did not extend across the entire width of the specimen. The crack spacing was between 210 and 850 μm; the average spacing for σ_a = 138 MPa was ~ 450 μm, and for σ_a = 100 MPa was ~ 470 μm. This observation suggests that the applied stress level has little effect on the crack spacing.

A polished cross section of the specimen (σ_a = 138 MPa) for the *x-z* plane is shown in Fig. 4b. Periodic segmentation of the ceramic layer (indicated by white arrows) is clearly observed, as expected from the cracking observed in the overall view of the specimen (Fig. 4a). Irregularly-shaped oxides are identified at the tips of blunt cracks in the ceramic (as indicated in Fig. 4a by the symbol "T"), which extend a short distance into the bond coat. This evidence suggests that these cracks are formed before final fracture of the specimen because formation of oxide on the new surface requires sufficient time at high temperature. An additional observation is that delamination at the interface between the oxide and ceramic, between adjacent through-thickness cracks in the ceramic, did not occur, indicating that cracking reduced the load bearing of the ceramic to effectively zero, with the added effect of mitigating the constraint of the ceramic on rumpling in the vicinity of the cracks.

Detailed observations of the polished cross sections demonstrate unique undulation behavior of the TGO layer (Fig. 5). The TGO layer in the y-z section shows clear rumpling similar to what has been observed in isothermal fatigue tests [18-19]. (Although most observations of TGO rumpling have been on PtNiAl bond coats, rumpling has also been observed in some instances on MCrAlY bond coats, e.g. [4]). However, the average undulation amplitude in the *x-z* section is much smaller compared to that in the *y-z* section, for both σ_a = 100 MPa and σ_a = 138 MPa; the *x-z* section is effectively planar whereas rumpling is clearly visible in the *y-z* section. One possible explanation is that through-thickness cracks that propagate through the TBC, as pictured in Fig. 5b, provide a stress relief mechanism for the TGO, by allowing the TGO to expand into the gaps created by cracks and opened further by the ratcheting strain. However, Fig. 5b also shows that these cracks do not form in the lower stress case, σ_a = 100 MPa, for the number of cycles shown, and yet the anisotropic rumpling behavior is still observed which rules out the aforementioned explanation. To investigate the undulation behavior in a quantitative manner, the wavelength ($2L$) and amplitude (2δ) of the TGO layer (Fig. 6) are assumed to have the following form:

$$w(x) = \delta(t)\cos(\pi x / L). \tag{2}$$

where $w(x)$ is the deflection of the midline of the TGO layer measured from the flat state (Fig. 6). The representation of the undulation given by Eq. (2), which describes the undulation in the x-direction, can also be used in the y-direction with δ and L interpreted as the corresponding quantities for an undulation in that direction (see Fig. 1a for the coordinate system). As will be demonstrated, the model equation for average stress through the thickness of the oxide in the x_1-direction (x-direction in the experiments) takes into account the Poisson effect caused by substrate constraint on mismatch strains in the x_3-direction (y-direction in the experiments), and vice versa. Therefore, the only assumption is that the morphology of the undulation in the x_1-direction does not directly affect or constrain the morphology in the x_3-direction, which is true for sufficiently small deformations; changes in undulation amplitude in the two directions are directly coupled through the oxide stress equations, which are the driving force for changes in undulation amplitude. The measured wavelengths and amplitudes are listed in Table 1 for the experiments depicted in Fig. 5. The wavelengths and amplitudes were obtained by fitting Eq. (2), in a least-squares sense, separately to 25 randomly selected bond coat/TGO interface profiles digitized from SEM images in each of the relevant directions (perpendicular and parallel to the loading axis), with the average of those 25 values of 2δ and $2L$ reported in Table 1 with their corresponding standard deviations. (Fitting instead to the upper surface of the TGO would give a slightly different result.) The wavelengths in the two directions are statistically the same, while the amplitudes are completely different as suggested by the polished sections in Fig. 5. (The images in Fig. 5 are each only one of the 25 profiles used to obtain the average values, hence only provide a qualitative indication of the large difference in the amplitude and relative similarity in the wavelength.) The amplitude perpendicular to the loading axis was much larger than in the parallel direction, and was larger (in terms of the average) for the lower of the two applied loads; the TGO layer was nearly flat in the loading direction after cycling. This result suggests that applied tensile loading at high temperature plays an important role in undulation behavior of the TGO layer, and further supports the idea that the TGO in-plane growth strain is the primary driving force for rumpling since the applied tensile stress in the parallel direction results in straining that mitigates the build up of compressive stress as a result of in-plane oxide growth. The anisotropic nature of the TGO undulation behavior and its applied stress dependence under in-phase TMF tests are the most important new findings obtained in the present work. The effect of both a thermal gradient and an axial tensile stress were recently reported in [24]. The model simulations point out that the axial stress causes

complicated undulation behavior influenced by many geometric and material parameters. The present study shows a clear TGO undulation trend associated with the applied stress by measuring systematically the undulation amplitudes and wavelengths.

3. TMF rumpling model

The boundary conditions assumed in an existing model of rumpling [12-13, 25] were adapted to the present case. The actual two-dimensional undulation pattern is approximated here by two one-dimensional undulations, although with direct coupling of the average stress through the oxide thickness in the two directions. The superalloy substrate is very thick relative to the layers above it, so all layers approximately experience the strain of the substrate during loading. Although the experiments were load-controlled, it is equivalent to model the boundary conditions as applied strain provided the actual measured strain cycle (Fig. 3b) is prescribed. Modeling the boundary conditions in this way does not require any consideration of the material behavior of the superalloy substrate, which experiences complicated ratcheting creep deformation under TMF conditions (see Fig. 3b). In the direction of applied loading, the measured substrate strain is $\dot{\varepsilon}_{11}^{(SUB)}$. Since temperature is changing in-phase with the applied loading, $\dot{\varepsilon}_{11}^{(SUB)}$ comprises contributions from both loading and thermal expansion. Only the part of the measured strain corresponding to loading leads to a Poisson contraction in the direction perpendicular to the loading. Therefore, in terms of the *measured* strain in the direction of applied loading, $\dot{\varepsilon}_{11}^{(SUB)}$, the strain experienced by the substrate in the direction perpendicular to the loading is:

$$\dot{\varepsilon}_{33}^{(SUB)} = -\nu^{(SUB)}\left(\dot{\varepsilon}_{11}^{(SUB)} - \alpha^{(SUB)}\dot{T}\right) + \alpha^{(SUB)}\dot{T}. \tag{3}$$

The following constitutive law is assumed for the bond coat (elasticity including thermal mismatch strain, and temperature-dependent power-law creep):

$$\dot{\varepsilon}_{ij}^{(BC)} = \frac{1+\nu^{(BC)}}{E^{(BC)}}\dot{\sigma}_{ij}^{(BC)} - \frac{\nu^{(BC)}}{E^{(BC)}}\dot{\sigma}_{kk}^{(BC)}\delta_{ij} + \left(\alpha^{(SUB)} - \alpha^{(BC)}\right)\dot{T}\delta_{ij} + \frac{3}{2}\dot{\varepsilon}_R^{(BC)}\,\mathrm{e}^{-T_R^{(BC)}/T}\left(\frac{\sigma_e^{(BC)}}{\sigma_R^{(BC)}}\right)^{n^{(BC)}-1}\frac{s_{ij}^{(BC)}}{\sigma_R^{(BC)}}, \tag{4}$$

where $\dot{\varepsilon}_R^{(BC)}$, $T_R^{(BC)}$ and $\sigma_R^{(BC)}$ are reference strain rate, temperature and stress, respectively, $n^{(BC)}$ is the power-law creep exponent, and $\sigma_e^{(BC)}$ and $s_{ij}^{(BC)}$ denote the effective stress and deviatoric stress tensor in the bond coat, respectively. Requiring that $\dot{\varepsilon}_{11}^{(BC)} = \dot{\varepsilon}_{11}^{(SUB)}$ and $\dot{\varepsilon}_{33}^{(BC)} = \dot{\varepsilon}_{33}^{(SUB)}$ leads to equations for the in- and out-of-plane stress in the bond coat (see [12, 25] for more explicit details on this approach):

$$\dot{\sigma}_{11}^{(BC)} = \bar{E}^{(BC)}\left[\left(1-\nu^{(SUB)}\nu^{(BC)}\right)\dot{\varepsilon}_{11}^{(SUB)} + \left[\left(1+\nu^{(SUB)}\right)\nu^{(BC)}\alpha^{(SUB)} - \left(1+\nu^{(BC)}\right)\alpha^{(BC)}\right]\dot{T}\right] - \bar{E}^{(BC)}\frac{3}{2}\dot{\varepsilon}_R^{(BC)}\left(\frac{\sigma_e^{(BC)}}{\sigma_R^{(BC)}}\right)^{n^{(BC)}-1}\frac{s_{11}^{(BC)} + \nu^{(BC)}s_{33}^{(BC)}}{\sigma_R^{(BC)}}\mathrm{e}^{-T_R^{(BC)}/T}, \quad (5)$$

$$\dot{\sigma}_{33}^{(BC)} = \bar{E}^{(BC)}\left[\left(\nu^{(BC)}-\nu^{(SUB)}\right)\dot{\varepsilon}_{11}^{(SUB)} + \left[\left(1+\nu^{(SUB)}\right)\alpha^{(SUB)} - \left(1+\nu^{(BC)}\right)\alpha^{(BC)}\right]\dot{T}\right] - \bar{E}^{(BC)}\frac{3}{2}\dot{\varepsilon}_R^{(BC)}\left(\frac{\sigma_e^{(BC)}}{\sigma_R^{(BC)}}\right)^{n^{(BC)}-1}\frac{\nu^{(BC)}s_{11}^{(BC)} + s_{33}^{(BC)}}{\sigma_R^{(BC)}}\mathrm{e}^{-T_R^{(BC)}/T}. \quad (6)$$

As in [12-13, 25], the oxide is assumed to be elastic/perfectly-plastic and has the usual contributions to average in-plane stress from in-plane oxide growth and change in undulation amplitude (the last two terms, respectively, in Eqns. (7) and (8)). Requiring further that $\dot{\varepsilon}_{11}^{(OX)} = \dot{\varepsilon}_{11}^{(SUB)}$ and $\dot{\varepsilon}_{33}^{(OX)} = \dot{\varepsilon}_{33}^{(SUB)}$ (again, the substrate is much thicker than the other layers, therefore applies its strain to those layers) leads to similarly modified (relative to [12-13, 25]) equations for the oxide stress:

$$\dot{\sigma}_{11}^{(OX)} = \bar{E}^{(OX)}\left[\left(1-\nu^{(SUB)}\nu^{(OX)}\right)\dot{\varepsilon}_{11}^{(SUB)} + \left[\left(1+\nu^{(SUB)}\right)\nu^{(OX)}\alpha^{(SUB)} - \left(1+\nu^{(OX)}\right)\alpha^{(OX)}\right]\dot{T}\right] - \bar{E}^{(OX)}\left[\left(1+\nu^{(OX)}\right)\dot{\varepsilon}_G - \frac{\pi^2\left(\delta_0+\delta\right)\dot{\delta}}{L^2}\right], \quad (7)$$

$$\dot{\sigma}_{33}^{(OX)} = \bar{E}^{(OX)}\left[\left(\nu^{(OX)}-\nu^{(SUB)}\right)\dot{\varepsilon}_{11}^{(SUB)} + \left[\left(1+\nu^{(SUB)}\right)\alpha^{(SUB)} - \left(1+\nu^{(OX)}\right)\alpha^{(OX)}\right]\dot{T}\right] - \bar{E}^{(OX)}\left[\left(1+\nu^{(OX)}\right)\dot{\varepsilon}_G - \frac{\pi^2\left(\delta_0+\delta\right)\dot{\delta}}{L^2}\right]. \quad (8)$$

It can be verified that Eqns. (5)-(8) simplify to those in [12-13, 25], as they must, when the axial strain consists only of thermal strain, i.e. $\dot{\varepsilon}_{11}^{(SUB)} = \dot{\varepsilon}_{33}^{(SUB)} = \alpha^{(SUB)}\dot{T}$. The undulation

growth rate formula initially derived in [12] by a linear perturbation analysis for an infinitely thick bond coat was later derived for a finite-thickness bond coat in [13]. However, it was demonstrated by comparing finite element calculations to the infinitely thick bond coat solution that the undulation growth rate does not depend on bond coat thickness (although it may do so indirectly in the general case through the effect of bond coat thickness on the in-plane stress that develops as a result of the substrate constraint) when the bond coat thickness is greater than the undulation wavelength; the finite element solution and the infinitely thick bond coat solution agreed when the bond coat thickness was greater than the undulation wavelength. This is to say that the stress and strain fields resulting from an undulation occurring at the top surface of the bond coat are decayed at the bottom surface when this condition is met. Here, the finite-thickness solution of [12] for the undulation amplitude growth rate, which is far simpler than the finite-thickness solution of [13], is used, since the thickness of the bond coat (≈ 150 μm) in the experiments was more than twice the wavelength of the undulations (Table 1):

$$\frac{\dot{\delta}}{L\dot{\varepsilon}_R^{(BC)}} = \left(\frac{p}{\sigma_R^{(BC)}}\right)\left[a\left(n^{(BC)},\sigma_s^{(BC)}\right)\left(\frac{\sigma_e^{(BC)}}{\sigma_R^{(BC)}}\right)^{n^{(BC)}-1} + b(n^{(BC)})\left|\frac{p}{\sigma_R^{(BC)}}\right|^{n^{(BC)}-1}\right], \tag{9}$$

where p is the sinusoidal pressure between the TGO and bond coat, a is the coefficient of the limiting solution for $\left|p/\sigma_e^{(BC)}\right| << 1$ obtained from the linear perturbation analysis in [12] and b is the coefficient of the limiting solution for $\left|p/\sigma_e^{(BC)}\right| >> 1$ obtained from finite element analysis in [12]. The stress ratio $\sigma_s^{(BC)}$ in a is $\sigma_{33}^{(BC)}/\sigma_{11}^{(BC)}$ for an undulation aligned with the loading and $\sigma_{11}^{(BC)}/\sigma_{33}^{(BC)}$ for an undulation in the direction perpendicular to the loading; b is not dependent on $\sigma_s^{(BC)}$ by virtue of the fact that $\left|p/\sigma_e^{(BC)}\right| >> 1$ for the solution involving b. The coefficients a and b from [12] are shown for the present situation:

$$a\left(n^{(BC)},\sigma_s^{(BC)}\right) = \frac{6n^{(BC)}\left[1-\sigma_s^{(BC)}\left(1-\sigma_s^{(BC)}\right)\right]\cos\left(\theta\left(n^{(BC)},\sigma_s^{(BC)}\right)/2\right)}{\pi\left[3+n^{(BC)}-4n^{(BC)}\sigma_s^{(BC)}\left(1-\sigma_s^{(BC)}\right)\right]}, \tag{10}$$

where

$$\theta\left(n^{(BC)},\sigma_s^{(BC)}\right)=\tan^{-1}\left(\frac{\sqrt{4-g^2\left(n^{(BC)},\sigma_s^{(BC)}\right)}}{g\left(n^{(BC)},\sigma_s^{(BC)}\right)}\right)+m\pi, \tag{11}$$

and

$$g\left(n^{(BC)},\sigma_s^{(BC)}\right)=\frac{3-n^{(BC)}-2n^{(BC)}\sigma_s^{(BC)}\left(1-\sigma_s^{(BC)}\right)}{n^{(BC)}\left(1-\sigma_s^{(BC)}\left(1-\sigma_s^{(BC)}\right)\right)}, \tag{12}$$

and

$$m=\begin{cases}1 & \text{if } n^{(BC)}>2 \text{ and } \dfrac{-\sqrt{3}\sqrt{n^{(BC)}-2}+\sqrt{n^{(BC)}}}{2\sqrt{n^{(BC)}}}<\sigma_s^{(BC)}<\dfrac{\sqrt{3}\sqrt{n^{(BC)}-2}+\sqrt{n^{(BC)}}}{2\sqrt{n^{(BC)}}}\\ 0 & \text{otherwise}\end{cases}, \tag{13}$$

and

$$b(n^{(BC)})=1.152-0.6117\cdot n^{(BC)}+0.1551\cdot n^{(BC)^2}-0.02081\cdot n^{(BC)^3}+0.001170\cdot n^{(BC)^4}. \tag{14}$$

The equation relating p to the stress and other parameters of the oxide layer, derived from a modified von Karman plate theory, is given in [12].

4. Model results and discussion

Simulations were carried out using the adapted rumpling model; the ceramic layer, while generally included in the model, is omitted here as in previous studies [12-13, 25]. The high temperature properties of the highly anisotropic ceramic layer are not well known, and the presence of a ceramic layer does not qualitatively affect the model predictions. Rumpling involves over 20 geometric, material and thermal history parameters. Thermal history and cyclic applied strain (corresponding to the applied load) were matched to the experiments. It has been established from previous simulations that as long as parameter values are within broadly sensible bounds, their exact values do not affect the trends predicted by the simulations. Consistency of predicted qualitative behavior between the model and experiments, over a broad range of different scenarios, suggests, if not proves, that the essential mechanics of rumpling is captured by the model, hence it can be used to study and understand the

mechanics of newly observed rumpling scenarios, as done here; this has been established by previous studies. Nevertheless, the parameters used here were chosen to match the experiments as carefully as possible given the available information. As characterizing the material properties for an entire TBC system over the temperature history it experiences is intractable for a single study, best available or typical values were used in the absence of data for this particular coating system (e.g. creep properties). Creep parameters used for the bond coat were consistent with [18], namely $\sigma_R^{(BC)} = 25$ MPa, $\dot{\varepsilon}_R^{(BC)} = 0.2$ s^{-1}, $n^{(BC)} = 4$, and $T_R^{(BC)} = 15{,}000$ K, and the temperature-dependent bond coat CTE consistent with [26] for a NiCoCrAlY γ-layer; the CTE varies quadratically with temperature from 12×10^{-6} °C^{-1} at 25 °C to 32×10^{-6} °C^{-1} at 1150 °C. Recent simulations [27] have shown that the CTE mismatch between the 5-10 μm upper layer of a dual-phase bond coat and the substrate is much more significant in rumpling than that of the remainder of the bond coat and the substrate, because the stress field induced by the traction applied at the surface of the bond coat by the undulating oxide layer decays rapidly with distance from the surface, hence the undulation is accommodated primarily by creep in the upper region of the bond coat. The variation in the CTE of the substrate with temperature was not measured experimentally. However, it can be extracted from the experimental strain cycles presented here by assuming a linear variation and matching

$$\varepsilon_{11}^{(SUB)} = \int_{T_L}^{T_P} \alpha^{(SUB)} dT = \int_{T_L}^{T_P} \left(\alpha_R + \frac{T - T_R}{T_P - T_R} (\alpha_P - \alpha_R) \right) dT , \qquad (15)$$

where the subscripts L, R and P denote the low temperature in the cycle, room temperature and the peak temperature in the cycle, respectively, to the strain experienced by the substrate during heat-up in the experiment (Fig. 3b). It should be noted that the heat-up strain was exactly the same for each cycle in the experiments, and there is no evidence of appreciable creep during the heat-up (thermal activation of creep is low except near the peak temperature, and the heating rate is fast which precludes creep), hence the omission of creep strain from Eq. (15) is justified. A typical room temperature thermal expansion coefficient for a Ni superalloy is roughly $\alpha_R = 12\times10^{-6}$ °C^{-1}. It was found using this simple inverse method, with $T_L = 300$ °C, $T_R = 25$ °C and $T_P = 1150$ °C that $\alpha_P = 17\times10^{-6}$ °C^{-1}. These values give excellent agreement between the strain predicted by Eq. (15) on the heat-up and cool-down parts of the thermal cycle and what was measured in the experiments, therefore it was concluded that the temperature variation of the CTE of the substrate was appropriately characterized in this way.

Other elastic properties of the layers were taken to be $\nu^{(SUB)} = 0.3$ ($E^{(SUB)}$ has no effect), $E^{(BC)} = 115$ GPa, $\nu^{(BC)} = 0.27$, $E^{(OX)} = 375$ GPa, $\nu^{(OX)} = 0.2$, and $\alpha^{(OX)} = 8.5\times10^{-6}$ °C^{-1}.

Wavelength and initial peak-to-peak undulation amplitude were taken to be 65 μm and 0.5 μm, respectively, the same for undulations in the direction of loading, and perpendicular to the direction of loading, consistent with the experiments. The initial oxide thickness was taken to be 1 μm, which presumes some high temperature exposure prior to cycling, e.g. during deposition of the ceramic layer. The oxide (Al_2O_3) yield stress was taken to be 300 MPa at 1150 °C with a temperature dependence matched to the measurements of Heuer et al. [28] for fine-grained Al_2O_3; a forthcoming plot of simulated oxide stress shows that yield occurs almost exclusively at the peak temperature, hence the temperature dependency of the oxide yield stress actually plays a very minor role. (The simulations always begin at 1150 °C with the stress in the oxide at -300 MPa, which presumes lateral growth straining to yield during the growth of the initial 1 μm oxide layer, during e.g. ceramic layer deposition, with all other layers stress-free.) Oxide thickening occurs consistent with the data of [29], according to an equation of the form:

$$\dot{h} = At^{-0.6}\exp\left(\frac{-Q}{kT}\right), \tag{16}$$

where $A = 1.12\times10^{13}$ μm·h$^{-0.4}$ (from a fit to the data of [29]), $Q = 3.96$ eV (from [30]) and $k = 8.62\times10^{-5}$ eV·K^{-1}; e.g. the oxide thickens from an initial value of 1 μm to 1.34 μm at the end of the 27 cycles described by Figs. 2 and 3. So-called lateral growth strain, which results from the kinetics of new oxide formation and is modeled as an in-plane expansion strain, occurs at a rate that is inversely proportional to the thickening rate, i.e. $\dot{\varepsilon}_G = \dot{h}/d$, where $d = 33.25$ m was chosen (d is a phenomenological parameter, having units of length, that does not have a particular physical significance), consistent with previous studies, such that 5% lateral growth strain would occur if the system were held for 100 hours at 1150 °C with the thickening rate given by (16); 1.03% lateral growth strain occurs over the 27 cycles described by Figs 2 and 3.

The measured cycle of strain in Fig. 3b was digitized and combined with the data in Fig. 3a to produce an accurate representation of the strain experienced by the substrate in the experiments, depicted in Fig. 7a. The magnitude of the strain change on heating and cooling is made constant in the idealized cycle in Fig. 7a, and substrate creep strain only occurs at the peak temperature. A through-thickness temperature gradient is not modeled, and in any case would have little effect as rumpling occurs roughly 200 μm from the top surface, compared to

the overall 3.35 mm thickness, hence the cyclic temperature is appropriately prescribed in accordance with the TBC temperature shown in Fig. 2. The thermal cycle used in the simulations, as in the experiments, is in-phase with the applied substrate strain. Undulation amplitude is plotted in Fig. 7b for 27 16-minute cycles with 3 minutes heating and cooling from room temperature and 10 minutes at the peak temperature, 1150°C. Details of how the simulations are carried out are given in [25].

As in the experiments, when subjected to the substrate strain of Fig. 7a, the model undulation perpendicular to the loading direction grows considerably (by nearly a factor of 4) and the undulation in the loading direction grows minimally and begins to flatten (see Fig. 7 insets) towards the end of the 27 cycles; the trends are the same between model and experiment and the final undulation amplitudes are also similar in the two directions after 27 cycles, although some suppression of rumpling by the ceramic layer not present in the model must occur prior to through-thickness cracking of the ceramic layer. It should be noted that no difference between in- and out-of-plane undulations is predicted by the previous set of model equations in which the substrate only undergoes thermal strain [12-13, 25]; the effect is a direct result of the anisotropy of the applied strain experienced by the substrate (which is transmitted to the layers attached to it), the effect of which can only be captured using the new model presented here.

The mechanism of undulation growth in the model is bond coat creep driven by the compressed oxide, facilitated by both thermal and stress activation of the creep mechanism, the latter resulting from strain mismatch between the bond coat and substrate [12-13, 25]. However, the effective stress in the bond coat, $\sigma_e^{(BC)} = \sqrt{\sigma_{11}^{(BC)^2} - \sigma_{11}^{(BC)}\sigma_{33}^{(BC)} + \sigma_{33}^{(BC)^2}}$, is unbiased towards in- and out-of-plane undulations and so anisotropy of the biaxial stress in the bond coat cannot be the cause of the observed undulation behavior since stress activation of creep is the same in both cases (thermal activation of creep is, of course, the same in the two directions); this is noteworthy as the degree of stress activation of creep in the bond coat, caused by mismatch strain with the substrate from a variety of sources, including thermal expansion mismatch, possible phase transformations and swelling caused by inter-diffusion with the substrate, has explained most other observed rumpling trends for PtNiAl bond coats. Examination of the stress in the oxide (Fig. 8) reveals the cause of the observed undulation behavior. Although oxide stress parallel to the loading direction begins in compression (due to the expansion strain that occurs during formation of the initial oxide layer), it experiences only tension at the peak temperature after just 6 cycles (Fig. 8a) as a result of the applied loading

(and its associated strain). In general (in the absence of applied loading), most undulation growth in oxide rumpling on PtNiAl bond coats occurs at the end of the heat-up and beginning of the isothermal period, when the creep mechanism is thermally activated and before the stress in the bond coat relaxes by creep (hence is stress activated) [12]. Although the oxide experiences compression at lower temperatures, this results in very little permanent undulation amplitude growth because the bond coat is resistant to creep at those temperatures. Tension, at or in the vicinity of the peak temperature, causes undulations to flatten (see inset Fig. 7b for parallel direction). On the contrary, Fig. 8b shows that the stress in the oxide perpendicular to the direction of loading is always compressive at elevated temperatures, causing undulations in that direction to grow (see inset Fig. 7b for perpendicular direction). In fact, because the Poisson's ratio of the superalloy is larger than that of the TGO, a Poisson effect causes further compression in the direction perpendicular to the loading, in addition to that caused by the lateral expansion (see Eq. (6)). Fig. 8b shows the oxide stress versus temperature for cycles 3 through 7 in the direction perpendicular to the loading, during which the stress transits from the compressive yield curve to the tensile yield curve. The effect of the substrate creep strain, applied to the layers above it at the peak temperature, is clearly evident. The oxide stress undergoes almost no permanent change as a result of heating followed by cooling. However, during the periods at the peak temperature, when the substrate creep strain is being applied, the oxide stress becomes incrementally larger, until, by the start of the peak temperature hold in cycle 7, the oxide stress has reached the tensile yield curve and thereafter remains tensile for all remaining cycles.

The experiments suggest that ratcheting observed in the cyclic substrate strain (Fig. 3b) is necessary to produce anisotropic undulation growth under TMF conditions. However, it is unclear from the present experiments whether the ratcheting strain is essential, or whether a comparable cyclic strain without ratcheting would qualitatively produce the same effect. To investigate this, a cycle of strain equivalent to the one in Fig. 7a during heating and cooling, but with substrate strain held constant at the peak temperature, is used for otherwise exactly the same simulations as depicted in Fig. 7b. Peak-to-peak amplitude is shown in Fig. 9 as a function of cycles for the applied strain shown in the lower inset of Fig. 9. The simulations show that undulations grow in directions both parallel and perpendicular to the loading, and that final undulation amplitudes are roughly the same for the two directions; there is no undulation flattening at high temperature in either case, indicating the stress in the oxide is compressive throughout the cycling (as an examination of the simulated oxide stress reveals),

although it decays very rapidly to nearly zero at the peak temperature (hence very little undulation growth occurs at the peak temperature). Therefore, the ratcheting strain is the cause of the anisotropic undulation patterns observed in the experiments. It is expected that strain controlled experiments (rather than stress controlled as carried out here) with no ratcheting strain would exhibit very little anisotropy in the undulation amplitude.

Although, for the cyclic applied tension case considered thus far, it is necessary to have ratcheting strain at the peak temperature for undulations to develop anisotropically, it is not the only applied stress history that can lead to anisotropic rumpling. For example, substrate strain cycles can be generated corresponding to constant applied tension and compression (i.e. constant throughout the entire history; no change with thermal cycling); anisotropic rumpling has been observed in PtNiAl bond coat systems subject to constant applied compression [31]. However, it is first necessary to deduce the creep properties of the substrate from the experimental strain cycle as follows. The entire thermal barrier (350 μm) is thin compared to the substrate (3 mm), therefore has little effect on the mechanical behavior of the substrate in response to uniaxial loading. Under this assumption, the strain rate of the substrate $\dot{\varepsilon}_{11}^{(SUB)}$ resulting from an applied load $\sigma_{11}^{(SUB)}$, assuming power-law creep is:

$$\dot{\varepsilon}_{11}^{(SUB)} = \alpha^{(SUB)}\dot{T} + \dot{\varepsilon}_R^{(SUB)}\, e^{-T_R^{(SUB)}/T} \left(\frac{\left|\sigma_{11}^{(SUB)}\right|}{\sigma_R^{(SUB)}} \right)^{n^{(SUB)}-1} \frac{\sigma_{11}^{(SUB)}}{\sigma_R^{(SUB)}}, \qquad (17)$$

Taking the substrate power-law creep exponent $n^{(SUB)} = 4$ and thermal activation $T_R^{(SUB)} = 15{,}000$ K to be the same as that used for the bond coat (from [18]), the value of $\dot{\varepsilon}_R^{(SUB)} \Big/ \left(\sigma_R^{(SUB)}\right)^{n^{(SUB)}}$ appropriate for the superalloy used in the experiments can be inferred by comparing a time integration of Eq. (17) with the first 15 cycles of the measured substrate strain shown in Fig. 3b. After 15 cycles, the degree of ratcheting observed at the peak temperature increases progressively from cycle to cycle, indicating a change to the creep properties of the material (see Fig. 3b); creep properties of the substrate here are based only on the first 15 cycles when the ratcheting is repeatable. The slope of the ratcheting strain at the peak-temperature was matched to that in Fig. 3b by choosing $\dot{\varepsilon}_R^{(SUB)} = 0.01$ s^{-1} and $\sigma_R^{(SUB)} = 86$ MPa (the combination is not unique). Using these creep parameters and the temperature dependence of the thermal expansion coefficient of the substrate derived previously, numerical integration of Eq. (17) matches perfectly with the measured substrate strain of Fig. 3b for the

first 15 cycles, hence these parameters can be regarded as a very good characterization of the actual power law creep behavior of the substrate.

The ratio of final undulation amplitude in the perpendicular direction to that in the parallel direction after 27 cycles for applied substrate strain cycles corresponding to $\sigma_{11}^{(SUB)}$ ranging between -180 MPa and 180 MPa, held constant throughout the thermal history, are shown in Fig. 10. The substrate strain cycles are generated by integrating Eq. (17) with constant $\sigma_{11}^{(SUB)}$ and temperature varying as in Fig. 2, with substrate creep and thermal expansion parameter as described previously. Rumpling is relatively isotropic for applied stress between -60 MPa and 60 MPa. The results show that applied *compression* leads to undulations aligning *parallel* to the direction of the loading, whereas applied *tension* leads to undulations aligning *perpendicular* to the direction of the loading. Compressive stress tends to increase undulation growth in whatever direction it is applied; as the thermal barrier coating is very thin compared to the substrate, the substrate carries essentially the entire load. The strain experienced by the substrate as a result of the applied load is transferred to the bond coat, increasing the effective stress in the bond coat, and is transferred to the oxide, amplifying the oxide compressive stress, or at least maintaining it at yield, and hence the driving force for rumpling. In addition, the compressive stress results in a Poisson expansion in the perpendicular direction that has the opposite effect on the oxide stress in that direction. Hence, compressive stress leads to increased undulation amplitude in the direction of loading, and decreased undulation amplitude in the direction perpendicular to the loading, both of which give rise to a decrease in the ratio $\delta_{\perp}/\delta_{\parallel}$. The effect of the Poisson expansion on limiting the growth of undulations in the perpendicular direction is actually the dominant effect on the behavior shown in Fig. 10 for sufficiently large applied compressive stress, simply because once sufficient compression is applied to maintain the compressive stress in the oxide at yield for the entirety of the high temperature exposure when the bond coat is susceptible to creep, further amplification of undulations in the direction parallel to the loading with further increase in the applied compression will not occur.

The effect when tension is applied is far more dramatic. Undulation growth parallel to the direction of the loading is increasingly inhibited without bound for applied tension greater than 60 MPa. The substrate creep that results at high temperatures from the applied tension is transferred to the oxide; the creep strain rate increases with increasing applied stress. The point at which the sharp increase in $\delta_{\perp}/\delta_{\parallel}$ shown in Fig. 10 occurs is when the creep strain rate

transferred to the oxide by the substrate begins to exceed the expansion strain in the oxide resulting from oxide growth, which generates the compressive stress in the oxide. As these strain rates are in opposing directions, the compressive stress in the oxide at high temperature decreases as applied tensile stress increases beyond roughly 60 MPa. This leads to a decrease in the undulation amplitude in the direction parallel to the loading. Opposite to the case of applied compression, the applied tension leads to a Poisson contraction in the perpendicular direction that leads to greater undulation growth in that direction. The combined effect is that undulations align perpendicular to the direction of applied loading, as in the TMF case. The alignment is dramatic for sufficiently large applied tensile stress, as the compressive stress in the oxide, the driving force for rumpling, becomes smaller and smaller. As shown in Fig. 10 by the open circle symbol, the stress in the oxide actually becomes tensile at high temperature for applied (constant) tensile stress greater than or equal to 180 MPa. In that case, undulations in the direction of the loading flatten.

Summary

It was observed from in-phase thermo-mechanical fatigue tests on an EB-PVD TBC system that TGO undulations exhibit clear anisotropic behavior under TMF conditions. It was found that the undulation wavelengths were nearly the same in both directions but the amplitude in the perpendicular direction was much larger than in the parallel direction. Simulations carried out using a now widely accepted model of TGO rumpling adapted to accommodate any loading scenario applied to the coating predict qualitatively and quantitatively similar behavior to the experiments. An explanation of the observed rumpling behavior based on the interplay between applied stress and the lateral expansion that occurs when new oxide forms follows directly from the model equations and simulations. The explanation gives further evidence that the lateral expansion strain in the TGO is the driving force for rumpling, and creep of the bond coat exacerbated by mismatch strain with the substrate is the accommodating mechanism. It was further concluded from the model simulations that the ratcheting strain experienced by the substrate during TMF, which is transferred to the coating, is essential for anisotropic undulation development under TMF. However, it was demonstrated with the model that constant applied stress also leads to anisotropic rumpling, with tension causing alignment in the perpendicular direction and compression causing alignment in the parallel direction.

Acknowledgements

This work was partially supported by the New Energy and Industrial Technology Development Organization (NEDO) under the “Nano-Coating Project.”

References

[1] Evans AG, Mumm DR, Hutchinson JW, Meier GH, Pettit FS. Prog Mater Sci 2001; 46:505.

[2] Tzimas E, Mullejans H, Peteves SD, Bressers J, Stamm W. Acta Mater 2000; 48:4699.

[3] Guo S, Kagawa Y. Surf Coat Tech 2004; 182:92.

[4] Shon YH, Kim JH, Jordan EH, Gell M. Surf Coat Tech 2001; 146-147:70.

[5] Mumm DR, Evans AG, Spitsberg IT. Acta Mater 2001; 49:2329.

[6] Schulz U, Menzebach M, Leyens C, Yang YQ. Surf Coat Tech 2001; 146-147:117.

[7] Xu T, He MY, Evans AG. Acta Mater 2003; 51:3807.

[8] Spitsberg IT, Mumm DR, Evans AG. Mater Sci Eng A 2005; 394:176.

[9] Kim SS, Liu YF, Kagawa Y. Acta Mater 2007; 55:3771.

[10] Mumm DR, Evans AG. Acta Mater 2000; 48:1815.

[11] Gell M, Jordan E, Vaidyanathan K, Mccarron K, Barber B, Shon YH, Tolpygo VK. Surf Coat Tech 1999; 120-121:53.

[12] Balint DS, Hutchinson JW. Acta Mater 2003; 51:3965.

[13] Balint DS, Xu T, Hutchinson JW, Evans AG. Acta Mater 2006; 54:1815.

[14] Tolpygo VK, Clarke DR. Acta Mater 2004; 52:5115.

[15] Tolpygo VK, Clarke DR, Murphy KS. Surf Coat Tech 2004; 188-189:62.

[16] Tolpygo VK, Clarke DR. Surface Coat Technol 2003; 163:81.

[17] Panat R, Hsia KJ. Rroc R Soc Lond. A 2004; 460:1957.

[18] Pan D, Chen MW, Wright PK, Hemker KJ. Acta Mater 2003; 51:2205.

[19] Taylor MP, Evans HE, Busso EP, Qian ZQ. Acta Mater 2006; 54:3241.

[20] Raffaitin A, Monceau D, Crabos F, Andrieu E. Scripta Mater 2007; 56:277.

[21] Maldini M, Harada H, Koizumi Y. Kobayashi T, Lupinc V. Scripta Mater 2003; 43:637.

[22] Reed RC, Cox DC, Rae CMF. Mater Sci Eng A 2007; 448:88.

[23] Xiao L, Chen DL, Chaturvedi MC. Mater Sci Eng A 2006; 437:157.

[24] Shi J, Karlsson AM, Baufeld B, Bartsch M. Mater Sci Eng A 2006; 434:39.

[25] Balint DS, Hutchinson JW. J Mech Phys Solids 2005; 53:949.

[26] Thomson RJ, Hemker KJ. Research to be published.

[27] Balint DS. Research to be published.

[28] Heuer AH, Tighe, NJ, Cannon, RM. J Am Ceram Soc 1980; 63:53.

[29] Tolpygo VK, Clarke DR. Acta Mater 2004; 52:5129.

[30] Grabke HJ, Steinhorst M, Brumm M, Wiemer D. Oxid Met 1991; 35:199.

[31] Dryepondt, S, Clarke, DR. Acta Mater 2009; 57:2321.

List of tables and figures

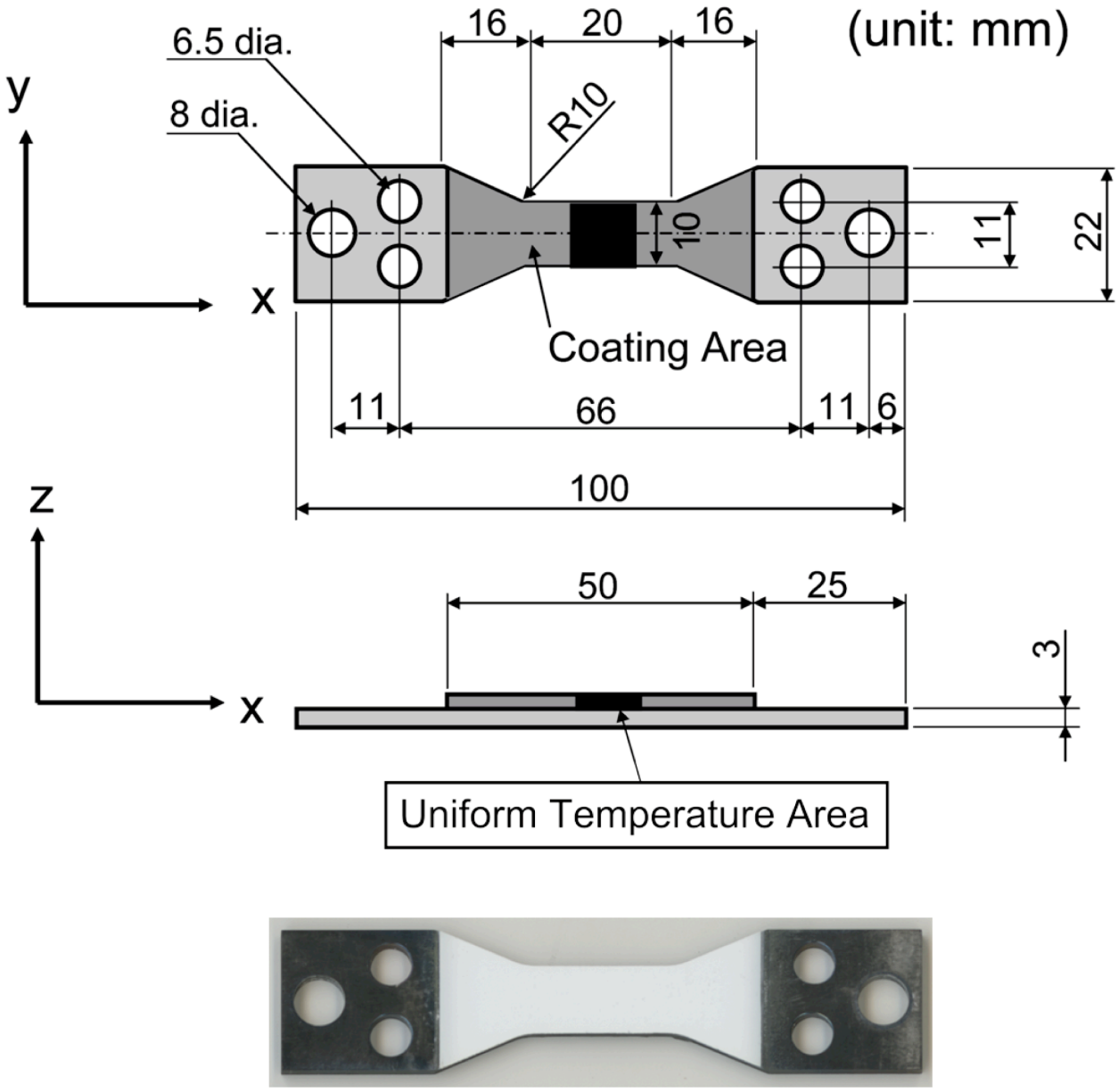

Fig. 1. (a) Shape and dimensions of the specimen.

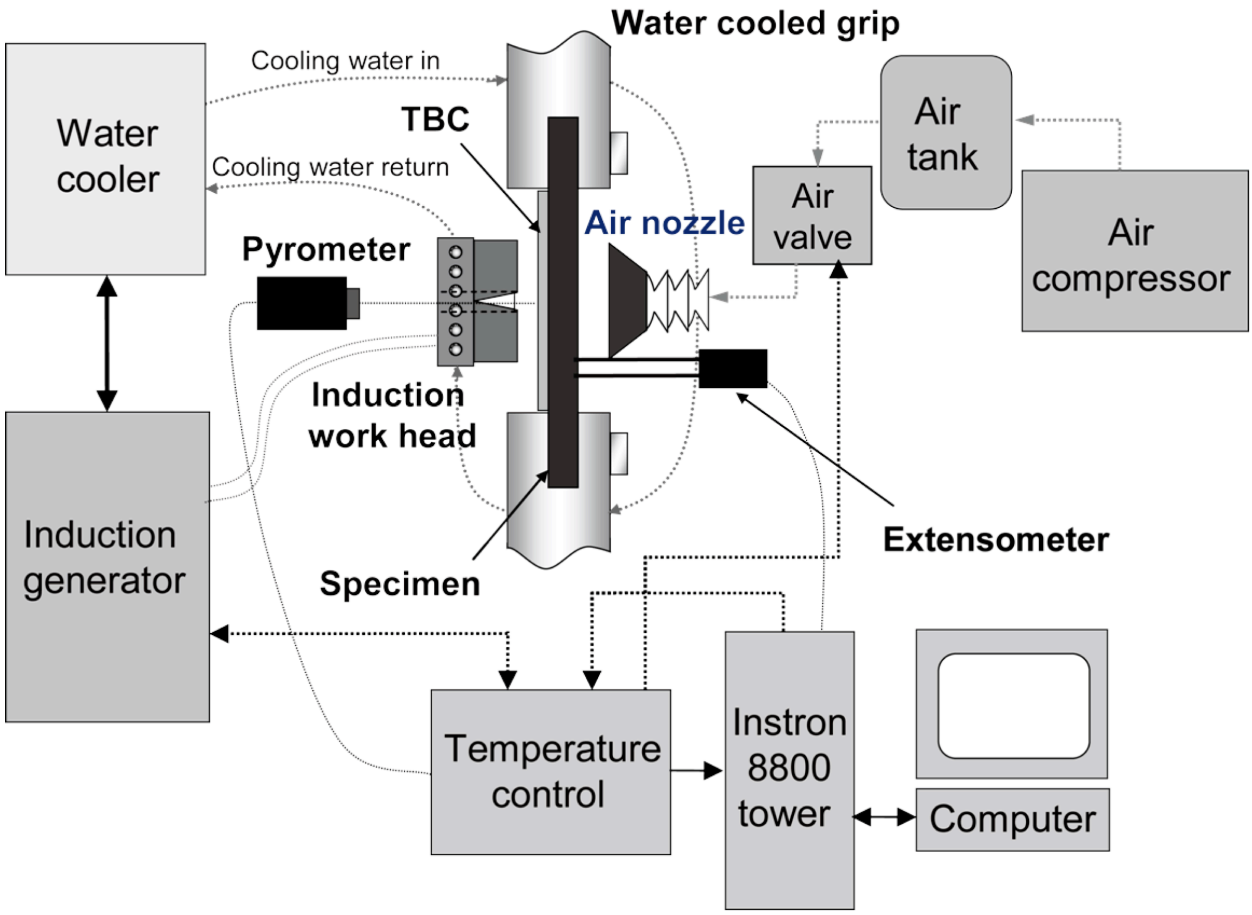

Fig. 1. (b) Setup of the TMF test.

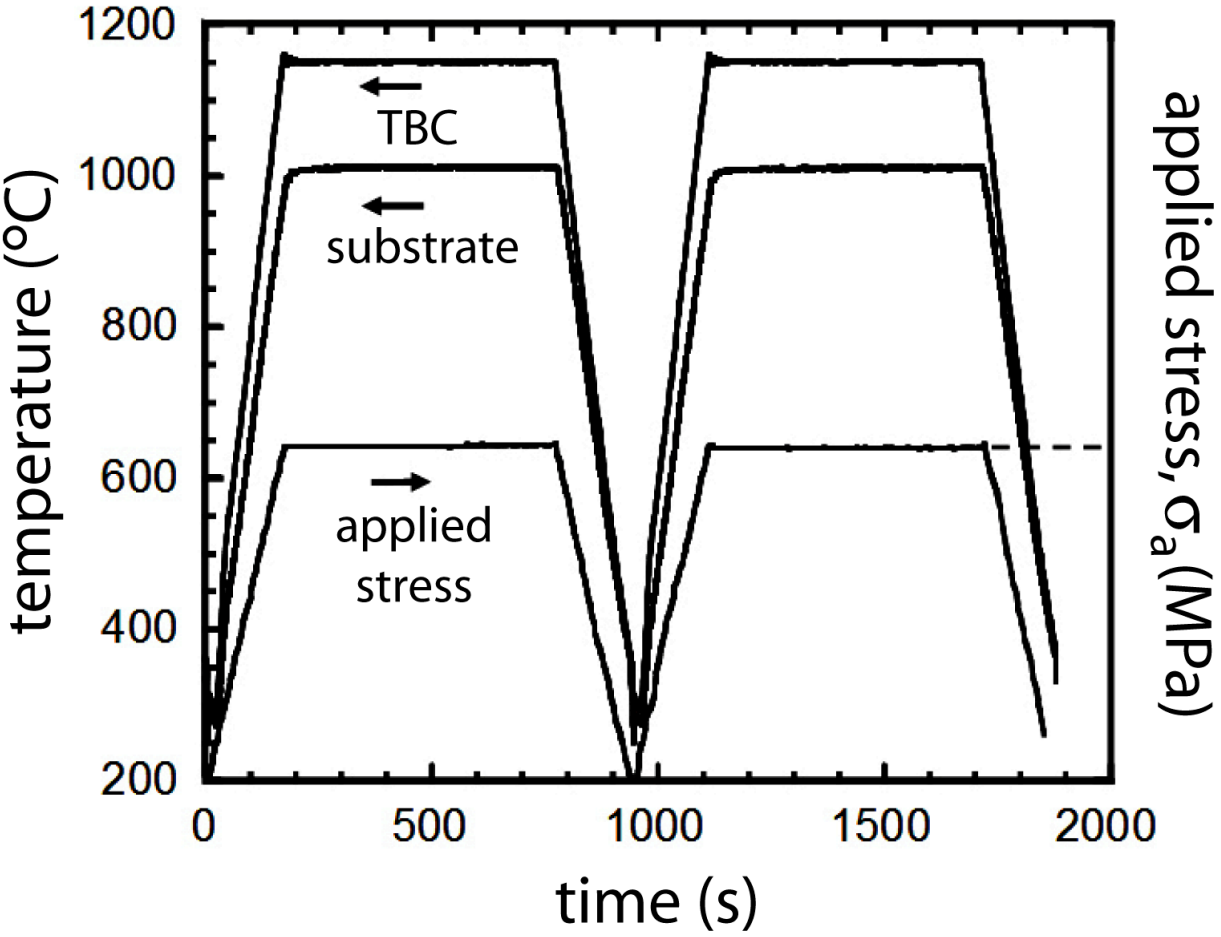

Fig. 2. An example of measured temperature-time and stress-time relations during the TMF test.

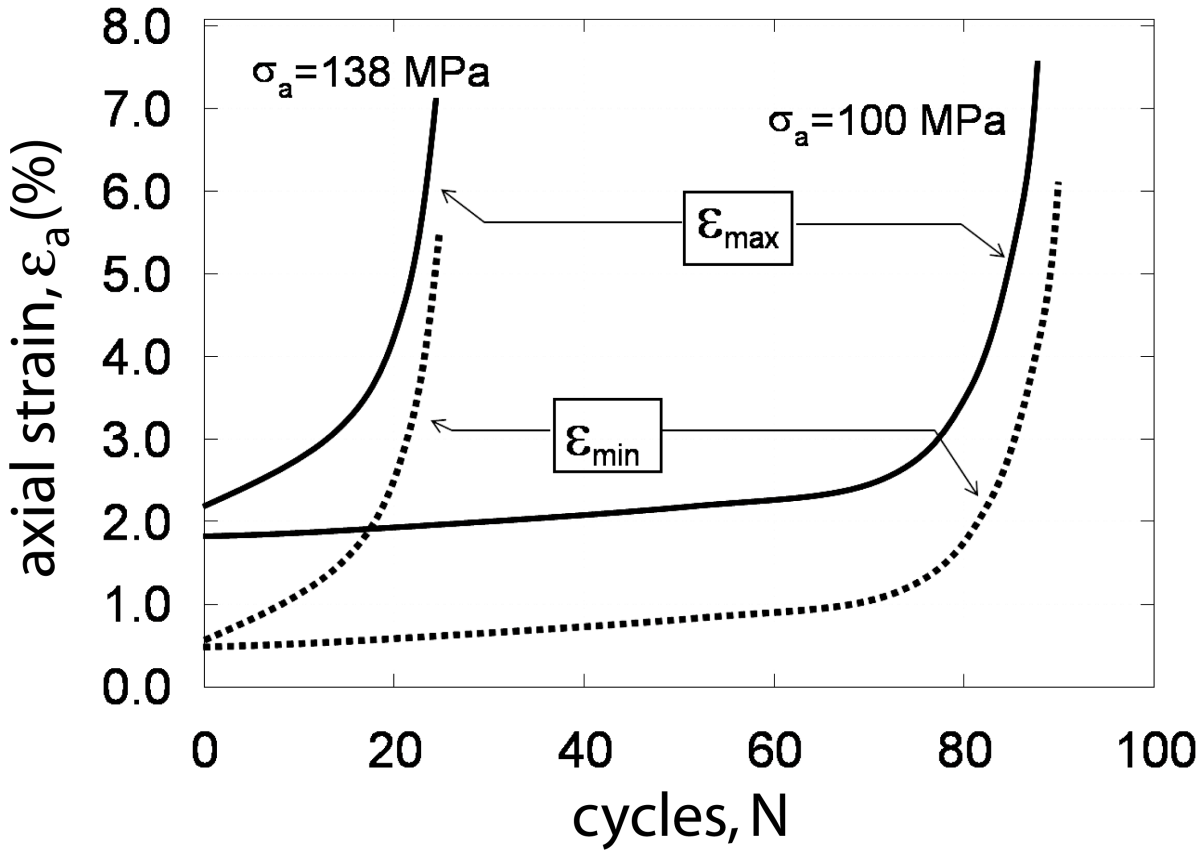

Fig. 3. (a) Accumulated maximum and minimum axial strains with increase in number of cycles *N* for σ_a = 138 and 100 MPa.

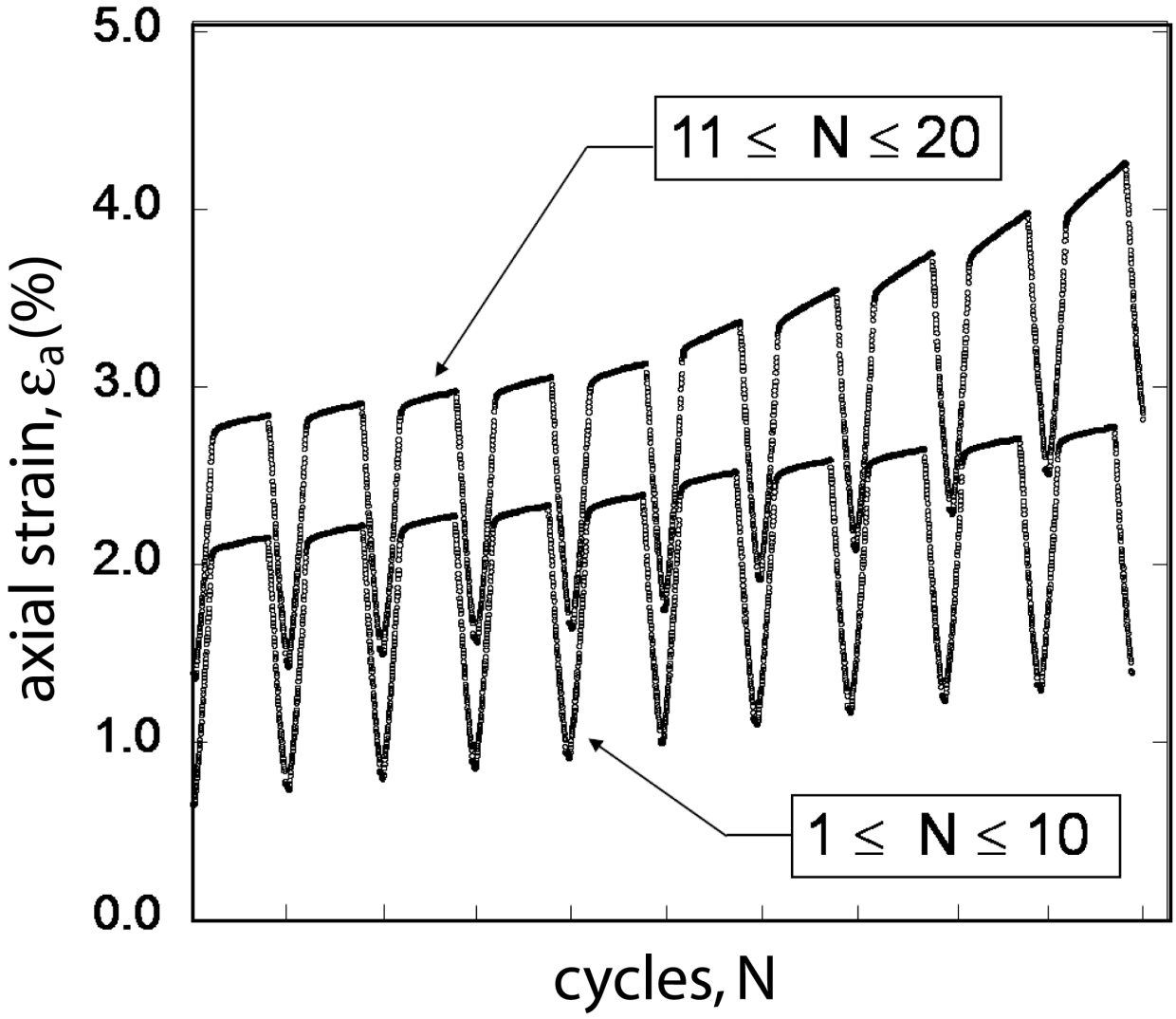

Fig. 3. (b) Cyclic axial strain versus number of cycles *N* for σ_a = 138 MPa.

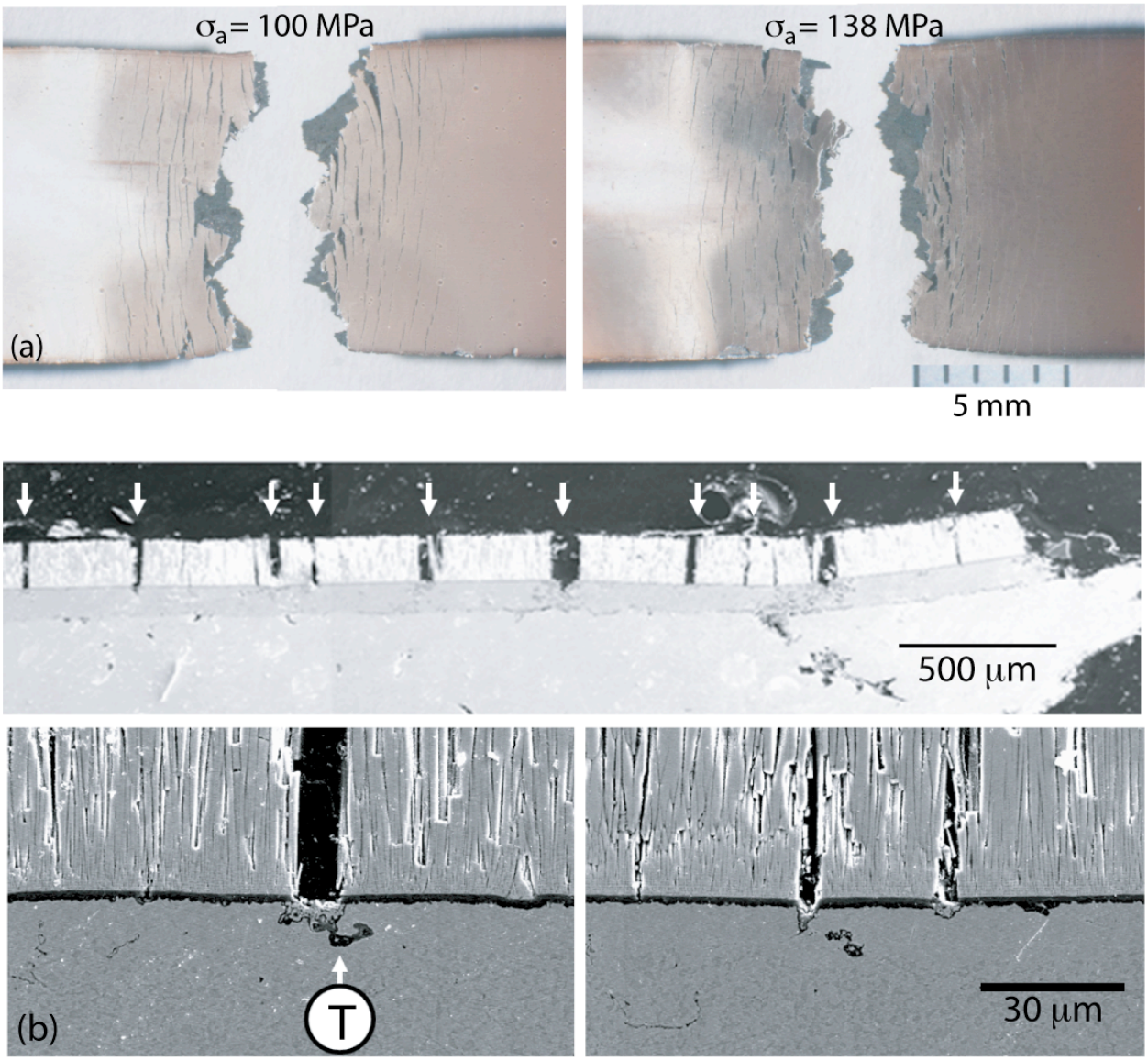

Fig. 4 (a) Overall view of tested specimens at final failure for σ_a = 138 and 100 MPa and (b) polished cross section of the σ_a = 138 MPa specimen for the x-z plane.

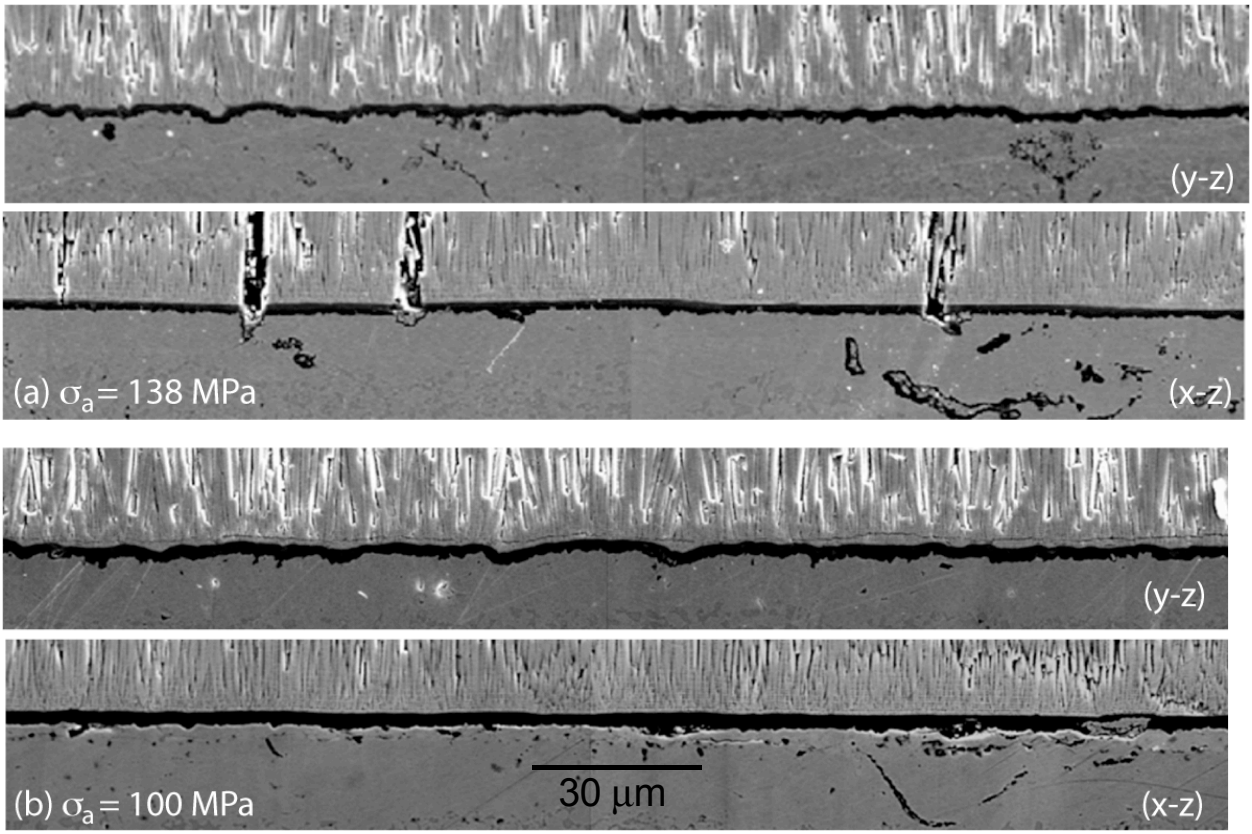

Fig. 5. Rumpling behavior of the TGO layer, for the directions perpendicular (y-z section) and parallel (x-z section) to the loading axis for (a) σ_a = 138 MPa and (b) σ_a = 100 MPa.

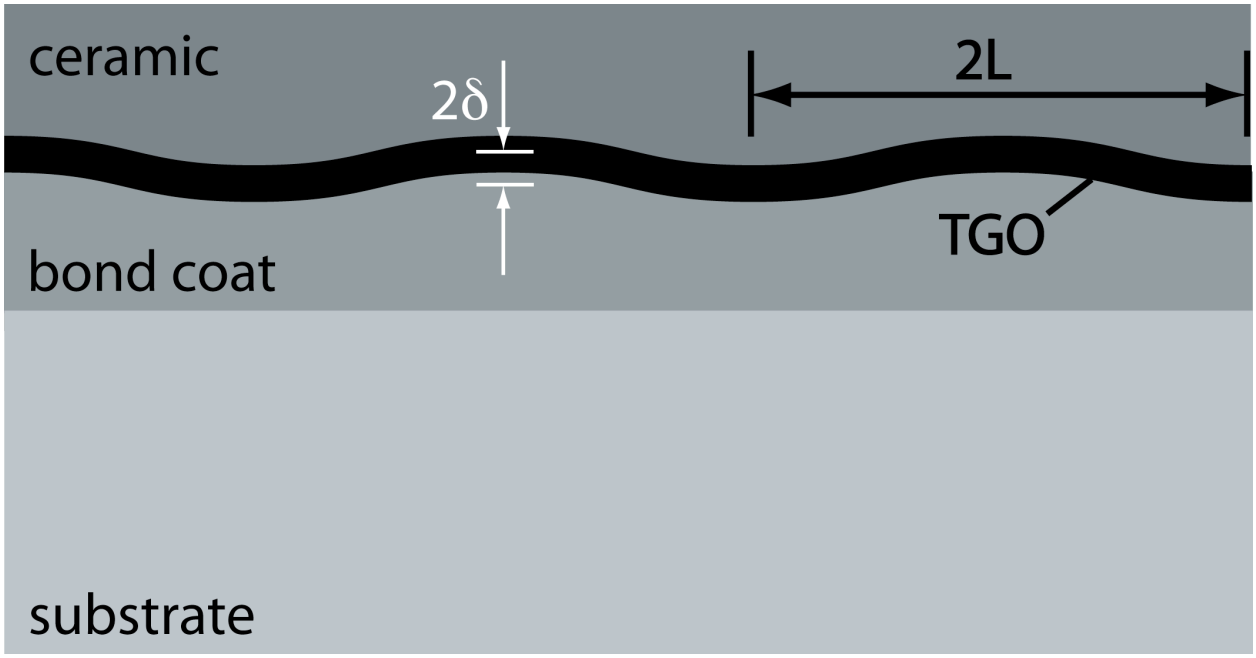

Fig. 6. Definition of undulation parameters: wavelength ($2L$) and peak-to-peak amplitude (2δ).

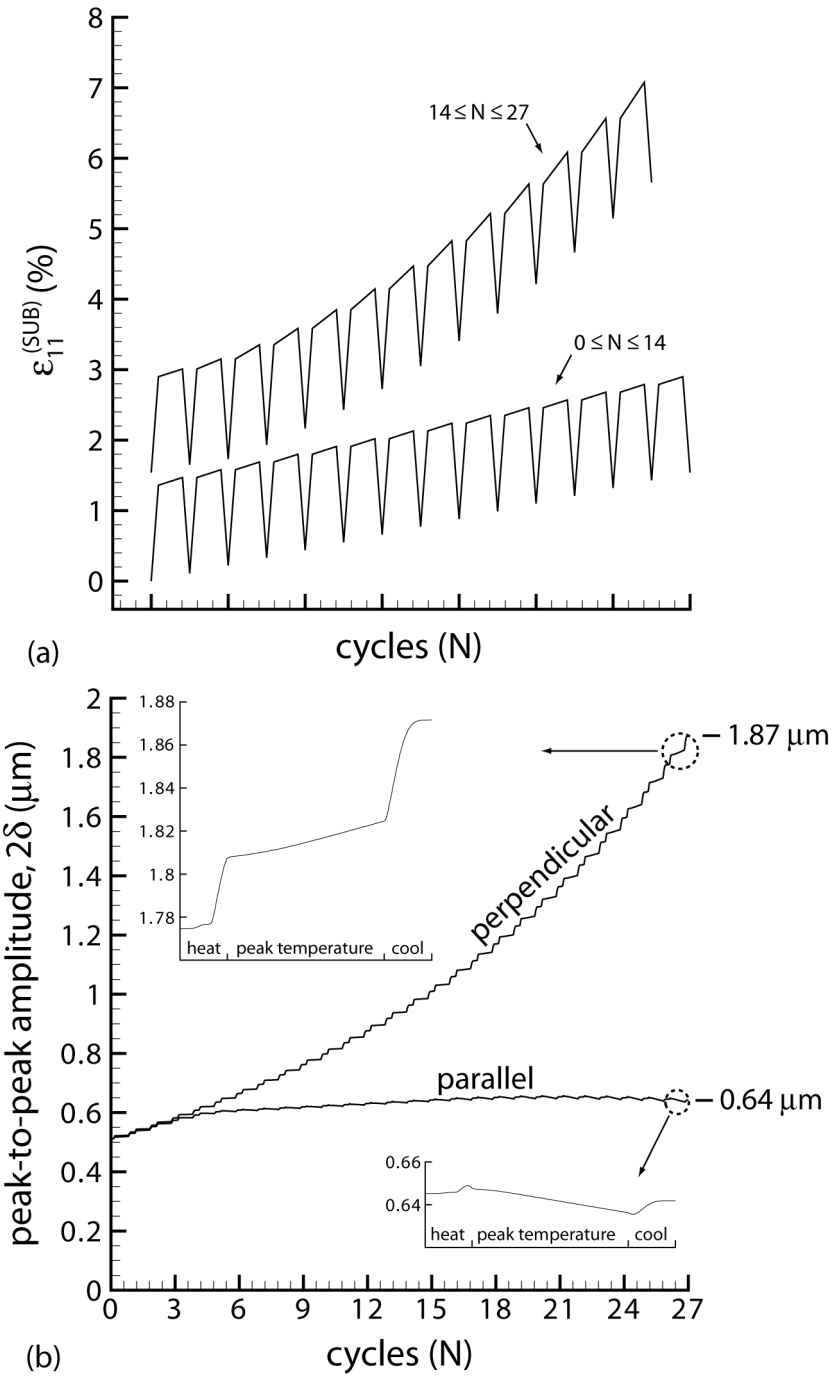

Fig. 7. (a) Idealized measured axial substrate strain applied in the model simulations and (b) peak-to-peak amplitude for undulations parallel and perpendicular to the loading direction with insets showing the final cycles magnified.

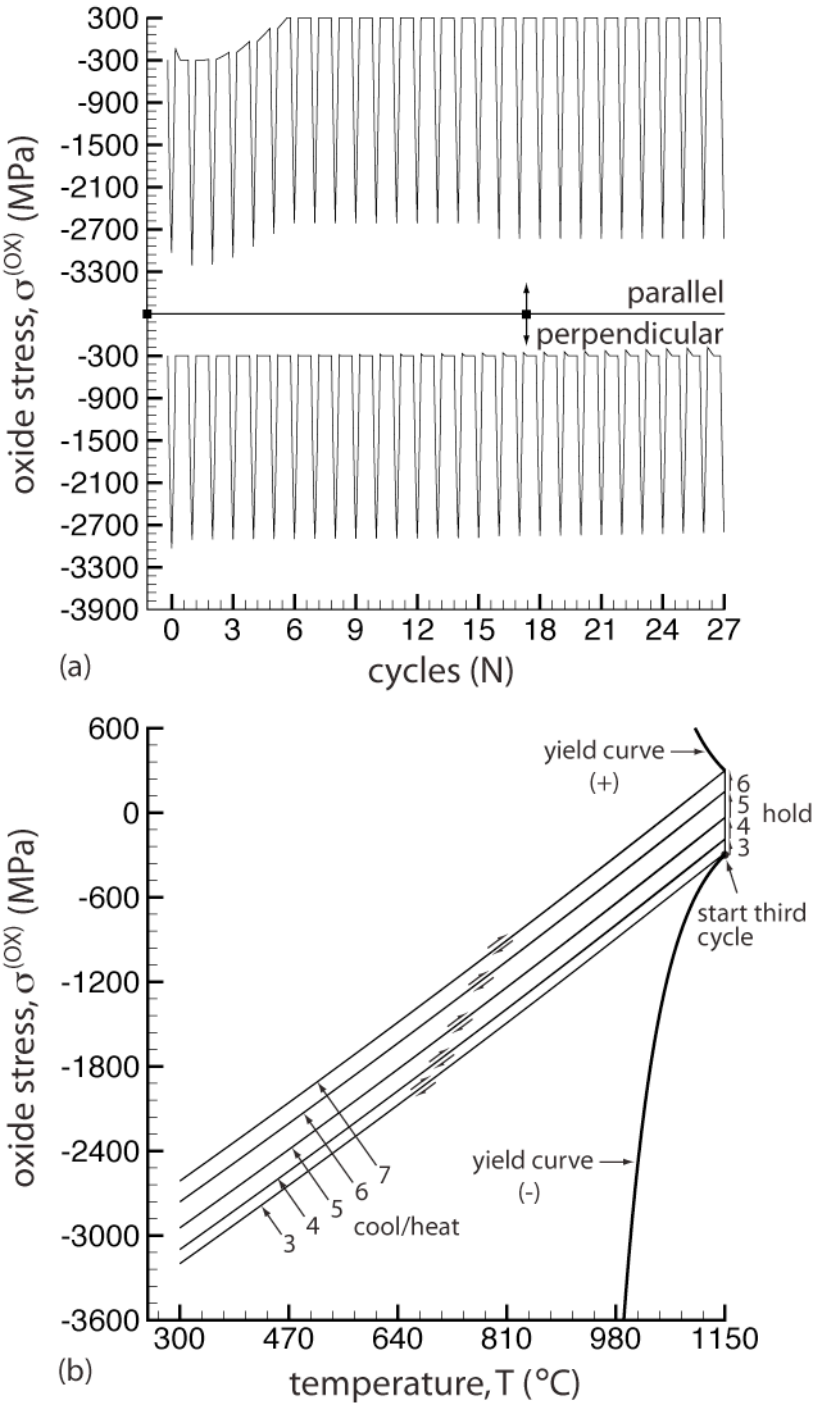

Fig. 8. Stress in the oxide (a) parallel to the direction of loading and (b) perpendicular to the direction of loading.

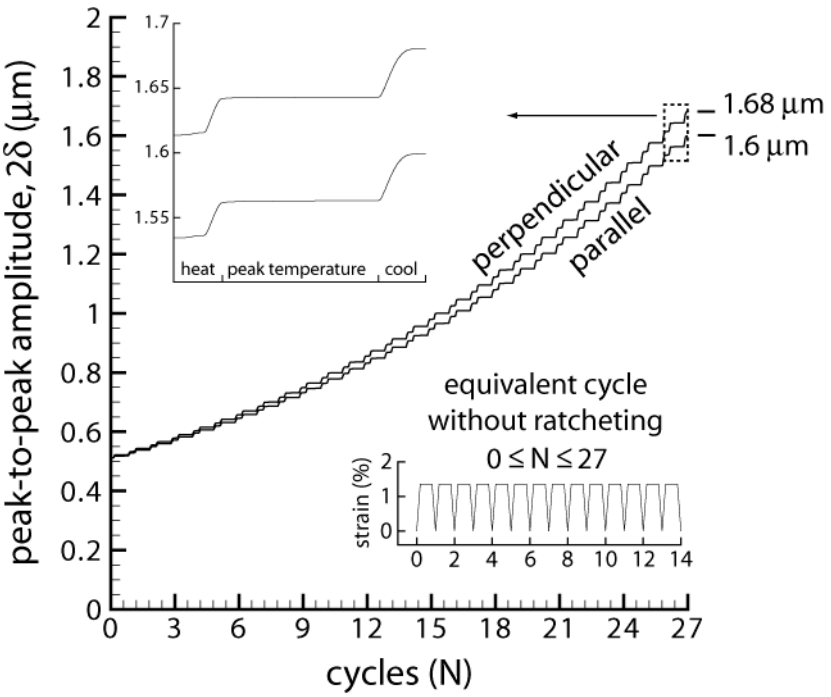

Fig. 9. Simulations as in Fig. 7b for the cycle of substrate strain shown in the lower inset, i.e. with substrate strain held constant at the peak temperature.

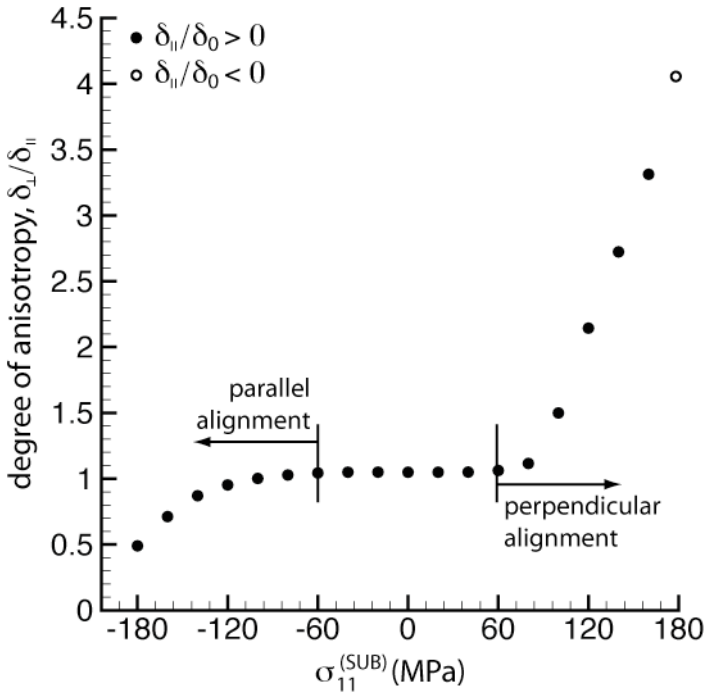

Fig. 10. Degree of undulation anisotropy versus constant stress applied to the coating.